The Journal of Infectious Diseases

MAJOR ARTICLE

Evidence of Severe Acute Respiratory Syndrome Coronavirus 2 Replication and Tropism in the Lungs, Airways, and Vascular Endothelium of Patients With Fatal Coronavirus Disease 2019: An Autopsy Case Series

Julu Bhatnagar,[1] Joy Gary,[1] Sarah Reagan-Steiner,[1] Lindsey B. Estetter,[1] Suxiang Tong,[2] Ying Tao,[2] Amy M. Denison,[1] Elizabeth Lee,[1] Marlene DeLeon-Carnes,[1] Yan Li,[2] Anna Uehara,[2] Clinton R. Paden,[2] Brooke Leitgeb,[1] Timothy M. Uyeki,[3] Roosecelis B. Martines,[1] Jana M. Ritter,[1] Christopher D. Paddock,[1] Wun-Ju Shieh,[1] and Sherif R. Zaki[1]

[1]Infectious Diseases Pathology Branch, Centers for Disease Control and Prevention, Atlanta, Georgia, USA, [2]Respiratory Viruses Branch, Centers for Disease Control and Prevention, Atlanta, Georgia, USA, and [3]Influenza Division, Centers for Disease Control and Prevention, Atlanta, Georgia, USA

Background. The coronavirus disease 2019 (COVID-19) pandemic continues to produce substantial morbidity and mortality. To understand the reasons for the wide-spectrum complications and severe outcomes of COVID-19, we aimed to identify cellular targets of severe acute respiratory syndrome coronavirus 2 (SARS-CoV-2) tropism and replication in various tissues.

Methods. We evaluated RNA extracted from formalin-fixed, paraffin-embedded autopsy tissues from 64 case patients (age range, 1 month to 84 years; 21 COVID-19 confirmed, 43 suspected COVID-19) by SARS-CoV-2 reverse-transcription polymerase chain reaction (RT-PCR). For cellular localization of SARS-CoV-2 RNA and viral characterization, we performed in situ hybridization (ISH), subgenomic RNA RT-PCR, and whole-genome sequencing.

Results. SARS-CoV-2 was identified by RT-PCR in 32 case patients (21 COVID-19 confirmed, 11 suspected). ISH was positive in 20 and subgenomic RNA RT-PCR was positive in 17 of 32 RT-PCR–positive case patients. SARS-CoV-2 RNA was localized by ISH in hyaline membranes, pneumocytes, and macrophages of lungs; epithelial cells of airways; and endothelial cells and vessel walls of brain stem, leptomeninges, lung, heart, liver, kidney, and pancreas. The D614G variant was detected in 9 RT-PCR–positive case patients.

Conclusions. We identified cellular targets of SARS-CoV-2 tropism and replication in the lungs and airways and demonstrated its direct infection in vascular endothelium. This work provides important insights into COVID-19 pathogenesis and mechanisms of severe outcomes.

Keywords. SARS-CoV-2; COVID-19; in situ hybridization; replication; autopsy.

Severe acute respiratory syndrome coronavirus 2 (SARS-CoV-2) emerged in Wuhan, China, in December 2019 and within a short time span spread worldwide, causing the coronavirus disease 2019 (COVID-19) pandemic [1, 2]. As of 30 January 2021, the COVID-19 pandemic has affected 222 countries, areas, or territories, leading to >101 million cases and >2.1 million deaths worldwide, including >435 000 deaths in the United States [2, 3]. As the COVID-19 pandemic continues to evolve, knowledge about its wide-spectrum clinical manifestations and disease-associated complications is advancing. Clinical manifestations range from mild respiratory symptoms to severe and fatal outcomes, including acute respiratory distress syndrome and multiorgan failure [4]. Evidence of additional COVID-19–associated complications, including frequent thromboembolic, cardiovascular, and neurological complications, is also emerging [4–9].

To understand the reasons for the wide-spectrum clinical manifestations, complications, and severe disease outcomes of COVID-19, it is critical to investigate cellular targets of SARS-CoV-2 tropism, replication, and mechanism of viral dissemination. Autopsy studies can be particularly valuable for answering these questions and providing deeper insight into the underlying pathophysiology of COVID-19. Previous autopsy studies have generally been limited to histopathological analysis and, if SARS-CoV-2–specific tissue-based assays were used, either they were restricted to specific organs or applied to specimens from a small case series of a specific geographic location [6, 8–19]. Although a few prior autopsy studies using immunohistochemistry are illustrative of distribution of SARS-CoV-2 antigens in tissues, the presence of antigens does not necessarily indicate virus replication [18, 19].

Received 7 December 2020; editorial decision 7 January 2021; accepted 22 January 2021; published online January 27, 2021.

Correspondence: Julu Bhatnagar, PhD, Infectious Diseases Pathology Branch, National Center for Emerging and Zoonotic Infectious Diseases, Centers for Disease Control and Prevention, 1600 Clifton Rd NE, Mailstop H18-SB, Atlanta, GA 30329-4027 (zrn1@cdc.gov).

The Journal of Infectious Diseases® 2021;XX:0–0

DOI: 10.1093/infdis/jiab039

The purpose of this work was to identify cellular targets of SARS-CoV-2 replication and tropism by directly localizing viral RNA in tissues from fatal COVID-19 patients, along with indicators of active viral replication, to better understand the severe disease outcomes, wide-spectrum complications, and viral pathogenesis. In addition, to identify the role of coinfections in severe outcomes and to detect alternate etiological pathogens, other respiratory pathogens were also evaluated. Here, we describe a comprehensive analysis of respiratory and nonrespiratory autopsy tissues from case patients with confirmed or suspected COVID-19, comprising both adult and pediatric patients who died after hospitalization or in community settings prior to any testing for SARS-CoV-2.

MATERIALS AND METHODS

Patient Specimens

Formalin-fixed, paraffin-embedded (FFPE) autopsy tissues from 64 case patients, including 21 with confirmed COVID-19 and 43 with suspected COVID-19, from 23 US states were evaluated. These specimens were submitted to the Infectious Diseases Pathology Branch, Centers for Disease Control and Prevention (CDC), Atlanta, Georgia, from local and state health departments, medical examiners, and pathologists between 23 January and 4 August 2020 for diagnostic consultation. This activity was reviewed by the CDC and was conducted consistent with applicable federal law and CDC policy (see 45 Code of Federal Regulations [CFR] part 46; 21 CFR part 56; 42 US Code [USC] §241(d); 5 USC §552a; 44 USC §3501 et seq.). All samples and associated medical and autopsy records were provided in the context of diagnostic consultation, a routine public health service provided by the CDC. As such, institutional review was not required for the testing described in this article. In this series, confirmed cases are defined as those with prior laboratory evidence of SARS-CoV-2 by respiratory swab RT-PCR; suspected cases had clinical or epidemiologic suspicion of COVID-19, but respiratory swab testing for SARS-CoV-2 was negative or not performed. FFPE respiratory tissues (lung, trachea, or bronchi) from all case patients and additional FFPE nonrespiratory tissues, including heart, brain, kidney, bladder, adrenal, thyroid, lymph nodes, liver, spleen, pancreas, gastrointestinal (GI), and urogenital tissues, as available, were evaluated by various assays. All tissues were analyzed by routine hematoxylin and eosin (H&E) staining to identify pathological changes. Clinical and histopathological findings from 9 case patients have been previously described [12, 19].

SARS-CoV-2 RT-PCR Assays and Sanger Sequencing

As a part of the ongoing COVID-19 response effort, we developed 2 conventional RT-PCR (cRT-PCR) assays for detection of SARS-CoV-2 in FFPE tissues, using the newly designed primers targeting the spike gene (*S*) and nucleocapsid gene (*N*), as described below: *S*-gene forward primer 5′-CTT CCC TCA GTC AGC ACC TC-3′; *S*-gene reverse primer 5′-GTT ACA AAC CAG TGT GTG CCA-3′; *N*-gene forward primer 5′-ACA TTG GCA CCC GCA ATC-3′; *N*-gene reverse primer 5′-TGA ACT GTT GCG ACT ACG TGA-3′. For validation, positive controls consisted of FFPE SARS-CoV-2 cultured cells while negative controls comprised of FFPE cell culture controls for alphacoronavirus (human coronavirus [HCoV] NL63), betacoronaviruses (HCoV-HKU1, Middle East respiratory syndrome coronavirus [MERS-CoV], severe acute respiratory syndrome coronavirus [SARS-CoV]) and FFPE tissues from RT-PCR–/PCR-confirmed cases of viral or bacterial infections, including influenza virus A and B, human parainfluenza virus 3, enterovirus, *Streptococcus pyogenes*, and *Streptococcus pneumoniae*.

RNA was extracted from FFPE tissues from all 64 case patients using RNA extraction protocol as previously described. [20] and evaluated by *N*-gene and *S*-gene cRT-PCR assays. The assays were performed using the OneStep RT-PCR Kit (Qiagen, Valencia, California) and 5 µL of RNA template, using the manufacturer's instructions. The thermocycling conditions for *N*-gene and *S*-gene RT-PCR assays were as follows: 1 cycle at 50°C for 30 minutes, 1 cycle at 95°C for 15 minutes, then 40 cycles of incubation at 94°C, 56°C, and 72°C for 1 minute each, followed by 1 cycle of final extension at 72°C for 10 minutes. The *N*-gene (150 bp) and *S*-gene (162 bp) PCR-positive amplicons were directly sequenced by Sanger sequencing on a GenomeLab GeXP sequencer (AB SCIEX, Redwood City, California). The search for homologies to known sequences was performed by using the BLAST nucleotide database (http://blast.ncbi.nlm.nih.gov/Blast.cgi). Validation results showed that the *S*-gene cRT-PCR was specific for SARS-CoV-2 while *N*-gene cRT-PCR amplified both SARS-CoV-2 and SARS-CoV controls. However, sequencing of amplicons clearly differentiated SARS-CoV-2 from SARS-CoV. A SARS-CoV-2–positive result was inferred only when an amplicon sequence showed ≥99% nucleotide identity with SARS-CoV-2.

To demonstrate evidence of active viral replication, an additional subgenomic RNA RT-PCR was performed on cRT-PCR–positive case patients, as described previously [21]. Additionally, SARS-CoV-2 real-time RT-PCR (rRT-PCR) assay was performed on tissues from cRT-PCR–positive case patients to evaluate cycle threshold (Ct) values for each tissue type for correlative assessment of viral load [22] (Supplementary Data).

RT-PCR and PCR Assays for Other Respiratory Pathogens

RNA extracts from FFPE respiratory tissues of 64 case patients were tested by rRT-PCR for influenza A and B viruses, respiratory syncytial virus, and human parainfluenza virus (HPIV) types 1–4, as previously described [23, 24]. DNA was extracted from FFPE respiratory tissues of case patients with clinical history and/or histopathology consistent with a possible respiratory bacterial infection and tested by PCR assays

for *S. pneumoniae*, *S. pyogenes*, *Streptococcus* species, and *Staphylococcus aureus*, and by wide-range eubacterial 16S rRNA gene PCR [25, 26].

In Situ Hybridization

Two ISH assays, using RNAscope probes (Advanced Cell Diagnostics, Newark, California) targeting the *N*- and *S*-genes of SARS-CoV-2, were developed and validated. For validation, positive controls consisted of FFPE SARS-CoV-2 cultured cells while negative controls comprised of FFPE cell culture controls for alphacoronavirus (HCoV-NL63), betacoronaviruses (HCoV-HKU1, MERS-CoV, SARS-CoV), and FFPE tissues from RT-PCR–confirmed cases of other viral infections, including influenza viruses A and B, HPIV-3, enterovirus, and Zika virus. To directly localize SARS-CoV-2 RNA in tissues, newly developed ISH assays were performed on respiratory and nonrespiratory tissues from 32 SARS-CoV-2 cRT-PCR–positive case patients, using the manufacturer's instructions (Advanced Cell Diagnostics). To further characterize specific cell types, ISH using RNAscope probes, including the *SFTPB* probe for type II pneumocytes, *CD68* for macrophages, and *MUC5B* and *MUC5AC* probes for goblet cells, were performed on serial sections from SARS-CoV-2 ISH-positive tissue blocks. ISH RNAscope probes targeting MERS-CoV and Zika virus were used as negative control probes on FFPE tissues from confirmed SARS-CoV-2 cases and cell cultures. The quality of RNA in tissues was assessed by using RNAscope human glyceraldehyde 3-phosphate dehydrogenase (GAPDH) probes.

Whole-Genome Sequencing

Whole-genome sequencing (WGS) was performed on available RNA extracts from FFPE tissues of SARS-CoV-2 cRT-PCR–positive case patients at the Respiratory Viruses Branch, CDC. The primary method utilized multiplex RT-PCR with a panel of overlapping sets of SARS-CoV-2 primers, employing either the Oxford Nanopore MinION or Illumina MiSeq sequencers [27]. Consensus sequences were generated with Minimap 2.17 and Samtools 1.9. Representative full-genome sequences with collection dates up until September 2020 were downloaded from GISAID for sequence analysis.

RESULTS

Case Patient Characteristics

Of all 64 case patients evaluated, the median age was 50 years (range, 1 month–84 years) and 54 (84%) were adults (≥18 years of age). Forty-seven (73%) had 1 or more underlying medical conditions. For those with known illness onset date available (n = 58), the median duration of illness (DOI) was 6 days (range, 0–40 days), and 34 (53%) died at home or in the emergency department. Demographic and clinical features of case patients are summarized in Table 1.

RT-PCR and PCR Findings

SARS-CoV-2 RNA was detected in respiratory tissues of 32 of 64 case patients by *N*-gene and *S*-gene cRT-PCR assays and sequencing of amplicons, showing 99%–100% nucleotide identity with SARS-CoV-2. SARS-CoV-2 cRT-PCR assays were positive in all 21 previously confirmed COVID-19 case patients and provided the first evidence of SARS-CoV-2 in 11 of 43 (26%) suspected COVID-19 case patients (Table 2), including the first 2 US COVID-19 deaths. Subgenomic RNA transcripts, indicating active SARS-CoV-2 replication, were detected by subgenomic RNA RT-PCR in lung or tracheal tissues of 17 of 32 (53%) cRT-PCR–positive case patients. In these 17 case patients, the DOI was 2–18 days. Additionally, our findings suggested a relationship between location of viral replication in respiratory tract tissues and DOI (Table 3). For instance, in a case patient (CP 12) with a 2-day DOI, replicative viral RNA was detected only in trachea, while in 4 case patients with DOI 7–18 days, replicative RNA was detected only in lung tissues. In addition, replicative viral RNA was detected in lung or trachea of 10 of 11 cRT-PCR–positive long-term care facility residents (DOI 2–18 days; median age, 74 years [range, 54–91 years]), indicating more extensive infection in this high-risk group of older patients with underlying conditions. Case-by-case results of all assays performed on cRT-PCR–positive case patients are summarized in Table 3.

SARS-CoV-2 tissue rRT-PCR was also positive for 30 of 32 (94%) cRT-PCR–positive case patients (Table 2). In general, lower Ct values (median Ct, 22.34 [range, 11.72–36.70; interquartile range {IQR}, 18.96–28.07]) were detected in lung (n = 30), in comparison to airways (median Ct, 29.08 [range, 17.55–36.04; IQR, 22.15–31.78]; n = 19), indicating higher viral load in lung tissues. Although both cRT-PCR and rRT-PCR were positive for heart, GI, kidney, brain, liver/spleen, or pancreas tissues for 14 (44%) case patients, SARS-CoV-2 rRT-PCR Ct values were generally higher for these, in comparison to respiratory tissues, suggesting lower viral load in nonrespiratory tissues (Supplementary Figure 3).

Coinfection of SARS-CoV-2 with other viral or bacterial pathogens, including influenza B, HPIV-3, *S. aureus*, and *S. pneumoniae*, were identified in respiratory tissues of 10 of 32 (31%) SARS-CoV-2 cRT-PCR–positive case patients (Tables 3 and 4). Other non–SARS-CoV-2 respiratory pathogens were also identified in respiratory tissues from 14 of 32 (44%) SARS-CoV-2 cRT-PCR–negative case patients (Table 4).

In Situ Hybridization and Histopathology Findings

SARS-CoV-2 ISH assays using *N*-gene and/or *S*-gene probes were performed on multiple FFPE tissues blocks from 32 cRT-PCR–positive case patients; 20 (63%) had at least 1 block of lung or trachea positive by ISH (Table 2). In the lungs, ISH staining demonstrating SARS-CoV-2 RNA was observed in hyaline membranes (Figure 1A and

Table 1. Demographic and Clinical Features of Case Patients

Characteristic	All Case Patients (N = 64)		Evidence of SARS-CoV-2 in Tissues (n = 32)		No Evidence of SARS-CoV-2 in Tissues (n = 32)	
Male	45	(70)	20	(63)	25	(78)
Age, median (range)	50 y (1 mo–84 y)		54 y (1 mo–84 y)		41 y (10 mo–73 y)	
Age, y						
<1	5	(8)	3	(9)	2	(6)
0–4	2	(3)	0	(0)	2	(6)
5–17	3	(5)	1	(3)	2	(6)
18–49	22	(34)	9	(28)	13	(41)
50–64	17	(27)	8	(25)	9	(28)
≥65	15	(23)	11	(34)	4	(13)
Underlying medical conditions	47	(73)	29	(91)	18	(56)
Cardiovascular disease	28	(44)	19	(59)	9	(28)
Diabetes	13	(20)	11	(34)	2	(6)
Obesity	22	(34)	13	(41)	9	(28)
Chronic kidney disease	12	(19)	11	(34)	1	(3)
ESRD requiring dialysis	4	(6)	4	(13)	0	(0)
Chronic liver disease	9	(14)	6	(19)	3	(9)
Chronic lung disease	14	(22)	8	(25)	6	(19)
Immunosuppression	7	(11)	5	(16)	2	(6)
Neurologic conditions	6	(9)	5	(16)	1	(3)
Other underlying medical conditions	4	(6)	2	(6)	2	(6)
Duration of illness, d, median (range) (n = 58)	6 (0–40)		7 (1–26)		5 (0–40)	
Location of death						
Home, ED, or other out-of-hospital location	34	(53)	16	(50)	18	(56)
Hospital	30	(47)	16	(50)	14	(44)
LTCF resident	11	(17)	11	(34)	0	(0)

Data are presented as No. (%) unless otherwise indicated.

Abbreviations: ED, emergency department; ESRD, end-stage renal disease; LTCF, long-term care facility; SARS-CoV-2, severe acute respiratory syndrome coronavirus 2.

1B), as well as within intra-alveolar cells, including alveolar macrophages and sloughed pneumocytes (Figure 1A2, 1 A4, and 1*B2*). Staining was also seen in pneumocytes lining alveoli (Figure 1A3 and 1A4) and in bronchiolar epithelium. Staining in pneumocytes and macrophages was determined by cell morphology, as well as by ISH staining for cell markers *SFTPB* and *CD68* in the serial sections of SARS-CoV-2–positive lung blocks (Supplementary Figure 2A1 and 2A2).

SARS-CoV-2 RNA was also observed in trachea/mainstem bronchi from 9 cRT-PCR–positive case patients, showing multifocal ISH staining in tracheal epithelium in both ciliated epithelial cells and goblet cells (Figure 2A2). Goblet cell staining was determined by cell morphology, as well as by cell marker for *MUC5B* and *MUC5AC* in serial sections of trachea (Supplementary Figure 2*A3* and 2*A4*). SARS-CoV-2 RNA was noted in the tracheal submucosal glands of 3 case patients (Figure 2A4). Multifocal ISH signals were also seen within

Table 2. Tissue-Based Severe Acute Respiratory Syndrome Coronavirus 2 Reverse-Transcription Polymerase Chain Reaction, In Situ Hybridization, and Whole-Genome Sequencing Results of Case Patients With Confirmed or Suspected Coronavirus Disease 2019

	COVID-19 Confirmed Case Patients (n = 21)		COVID-19 Suspected Case Patients (n = 43)		Total No. of Case Patients (n = 64)	
Tissue-Based SARS-CoV-2 Assay	Cases Tested, No.	Positive, No. (%)	Cases Tested, No.	Positive, No. (%)	Cases Tested, No.	Positive, No. (%)
SARS-CoV-2 conventional RT-PCR	21	21 (100)	43	11 (26)	64	32 (50)
SARS-CoV-2 real-time RT-PCR[a]	21	20 (95)	11	10 (91)	32	30 (94)
Subgenomic RNA RT-PCR[a]	21	15 (71)	11	2 (18)	32	17 (53)
SARS-CoV-2 ISH[a]	21	16 (76)	11	4 (36)	32	20 (63)
WGS (full/partial)[a,b]	20	19 (95)	7	7 (100)	27	26 (96)

Abbreviations: COVID-19, coronavirus disease 2019; ISH, in situ hybridization; RT-PCR, reverse-transcription polymerase chain reaction; SARS-CoV-2, severe acute respiratory syndrome coronavirus 2; WGS, whole-genome sequencing.

[a]ISH, real-time RT-PCR, subgenomic RNA RT-PCR, and WGS were performed only on case patients with conventional RT-PCR–positive results.

[b]WGS was not performed on 5 case patients due to poor RNA quality or unavailability of specimens.

Table 3. Characteristics and Laboratory Findings of Case Patients With Evidence of Severe Acute Respiratory Syndrome Coronavirus 2 by Tissue Analysis

				SARS-CoV-2 Tissue-Based Testing											
				Conventional RT-PCR (*N*-Gene and *S*-Gene)		Real-time RT-PCR (*N*-Gene)		Subgenomic RNA RT-PCR		ISH Staining (*N*-Gene and/or *S*-Gene)		WGS Genome (%)/ Mutation			
Case Patient No.	Age	Duration of Illness, d	LTCF Resident	Trachea	Lung	Trachea Ct	Lung Ct	Trachea	Lung	Trachea	Lung		SARS-CoV-2 Respiratory Swab RT-PCR	Histopathology Findings (Lung and/or Airways)	Bacterial/Viral Coinfection
1	52	13	No	Positive	Positive	30.1	27.81	Negative	Positive	Negative	Positive	Full/D614G	Positive	Tracheobronchitis, DAD	Not detected
2	45	Unknown	No	NA	Positive	NA	15.39	NA	Positive	NA	Positive	Full/D614G	Positive	DAD, interstitial pneumonitis, fibrin thrombi	Not detected
3	91	8	Yes	Positive	Positive	21.39	17.27	Positive	Positive	Positive	Positive	Full/D614G	Positive	Tracheobronchitis, DAD, fibrin thrombi	Not detected
4	<1	3	No	NA	Positive	NA	No Ct	NA	Negative	NA	Negative	ND	Positive	Interstitial pneumonitis	Not detected
5	54	19	No	Negative	Positive	No Ct	27.49	ND	Negative	Negative	Negative	Not obtained	Positive	Tracheobronchitis, DAD, bronchopneumonia	Not detected
6	45	18	No	Positive	Positive	34.3	21.77	Negative	Positive	Negative	Positive	Full/D614G	Positive	Tracheobronchitis, DAD	Not detected
7	82	19	Yes	Positive	Positive	35.33	34.37	Negative	Negative	Negative	Negative	Partial (85)	Positive	Tracheobronchitis, fibrin thrombi	Not detected
8	59	17	No	Positive	Positive	29.92	20.81	Negative	Positive	Positive	Positive	Full/D614G	Positive	DAD, bronchopneumonia	Not detected
9	17	1	No	Positive	Positive	31.24	24.2	Negative	Negative	Negative	Negative	Partial (87)/ D614G	Positive	Tracheobronchitis, pulmonary hemorrhage	Not detected
10	<1	1	No	Negative	Positive	No Ct	29.54	ND	Negative	Negative	Negative	Partial (49)	Positive	Pulmonary edema	Not detected
11	35	7	No	Positive	Positive	32.31	21.49	Negative	Positive	Negative	Positive	Full	Positive	DAD	Not detected
12	64	2	Yes	Positive	Positive	17.55	28.85	Positive	Negative	Positive	Negative	Full/D614G	Positive	Tracheobronchitis, bronchopneumonia	Not detected
13	74	7	Yes	Positive	Positive	18.44	13.81	Positive	Positive	Positive	Positive	Full	Positive	Tracheobronchitis, DAD	HPIV-3
14	54	12	Yes	Positive	Positive	28.11	22.01	Positive	Positive	Positive	Positive	Full	Positive	Tracheobronchitis, bronchopneumonia, fibrin thrombi	*Streptococcus* spp
15	74	11	Yes	Positive	Positive	22.9	20.29	Positive	Positive	Positive	Positive	Full	Positive	Tracheobronchitis, DAD, interstitial pneumonitis	HPIV-3
16	84	16	Yes	Positive	Positive	17.58	14.61	Positive	Positive	Positive	Positive	Full	Positive	Tracheobronchitis, DAD, bronchopneumonia	*Streptococcus* spp
17	71	13	Yes	Positive	Positive	19.8	11.72	Positive	Positive	Positive	Positive	Full	Positive	Tracheobronchitis, DAD, bronchopneumonia, interstitial pneumonitis	*Streptococcus* spp
18	75	5	Yes	Positive	Positive	24.23	14.2	Positive	Positive	Positive	Positive	Full	Positive	Tracheobronchitis, DAD, bronchopneumonia	Not detected
19	57	10	Yes	Positive	Positive	33.55	22.95	ND	Positive	Negative	Positive	Full	Positive	Tracheobronchitis, DAD	Not detected
20	73	13	Yes	Positive	Positive	24.6	22.67	Positive	Positive	Negative	Positive	Full	Positive	Tracheobronchitis, DAD	Influenza B
21	52	26	No	Negative	Positive	No Ct	26.7	Negative	Negative	Negative	Positive	Partial (60)	Positive	Tracheobronchitis, DAD, fibrin thrombi	*Staphylococcus aureus*/ MSSA
22	47	7	No	NA	Positive	NA	19.59	NA	Negative	NA	Positive	Full/D614G	ND	DAD, bronchopneumonia, fibrin thrombi	*Streptococcus pneumoniae*

Table 3. Continued

				SARS-CoV-2 Tissue-Based Testing											
				Conventional RT-PCR (*N*-Gene and *S*-Gene)		Real-time RT-PCR (*N*-Gene)		Subgenomic RNA RT-PCR		ISH Staining (*N*-Gene and/or *S*-Gene)		WGS Genome (%)/ Mutation			
Case Patient No.	Age	Duration of Illness, d	LTCF Resident	Trachea	Lung	Trachea Ct	Lung Ct	Trachea	Lung	Trachea	Lung		SARS-CoV-2 Respiratory Swab RT-PCR	Histopathology Findings (Lung and/or Airways)	Bacterial/Viral Coinfection
23	45	1	No	NA	Positive	NA	19.48	NA	Negative	NA	Positive	Partial (70)/ D614G	ND	DAD, bronchopneumonia, fibrin thrombi	*Serratia* spp, *Haemophilus* spp
24	27	Unknown	No	NA	Positive	NA	31.29	NA	Negative	NA	Positive	ND	Negative	Pulmonary hemorrhage, capillaritis	Not detected
25	38	2	No	Positive	Positive	36.04	36.7	Negative	Negative	Negative	Negative	ND	Negative	DAD, bronchitis, fibrin thrombi	Not detected
26	<1	2	No	NA	Positive	NA	31.9	NA	Negative	NA	Negative	ND	ND	Tracheobronchitis, mild hemorrhage	Not detected
27	35	4	No	NA	Positive	NA	No Ct	NA	Negative	NA	Negative	ND	ND	DAD, bronchopneumonia.	*Streptococcus* spp
28	69	5	No	Positive	Negative	30.31	No Ct	Negative	Negative	Negative	Negative	Partial (78)	Indeterminate	Autolysis	Not detected
29	57	3	No	Positive	Positive	29.08	29.21	Negative	Negative	Negative	Negative	Partial (68)	ND	Tracheobronchitis, interstitial pneumonitis	Not detected
30	72	3	No	NA	Positive	NA	17.4	NA	Positive	NA	Positive	Full	ND	DAD, interstitial pneumonitis	Not detected
31	76	Unknown	No	NA	Positive	NA	26.14	NA	Positive	NA	Negative	Full	Negative	Emphysematous changes	Not detected
32	36	17	No	Negative	Positive	ND	31.07	Negative	Negative	Negative	Negative	Full	ND	Tracheobronchitis, DAD	Not detected

Abbreviations: Ct, cycle threshold; DAD, diffuse alveolar damage; HPIV, human parainfluenza virus; ISH, in situ hybridization; LTCF, long-term care facility; MSSA, methicillin-susceptible *Staphylococcus aureus*; NA, not available; ND, not done; RT-PCR, reverse-transcription polymerase chain reaction; SARS-CoV-2, severe acute respiratory syndrome coronavirus 2; WGS, whole-genome sequencing.

Table 4. Reverse-Transcription Polymerase Chain Reaction (RT-PCR) or PCR Results for Other Respiratory Pathogens Among Severe Acute Respiratory Syndrome Coronavirus 2 Tissue RT-PCR–Positive and –Negative Case Patients

	SARS-CoV-2 Tissue Conventional RT-PCR			
	Positive (n = 32)		Negative (n = 32)	
Tissue-Based RT-PCR or PCR for Other Respiratory Pathogens	Cases Tested, No.	Positive, No. (%)	Cases Tested, No.	Positive, No. (%)
Influenza virus RT-PCR[a]	32	1 (3)	32	7 (22)
Human parainfluenza virus RT-PCR[a]	32	2 (6)	32	3 (9)
Respiratory syncytial virus RT-PCR[a]	32	0 (0)	32	2 (6)
Streptococcus pyogenes PCR[b]	0	0 (0)	3	3 (100)
Streptococcus pneumoniae PCR[b]	10	1 (10)	3	0 (0)
Streptococcus spp PCR[b]	10	4 (40)	3	1 (33)
Staphylococcus aureus PCR[b]	1	1 (100)	6	5 (83)
Wide-range eubacteria PCR[b]	6	1 (17)	0	0 (0)

Abbreviations: PCR, polymerase chain reaction; RT-PCR, reverse-transcription polymerase chain reaction; SARS-CoV-2, severe acute respiratory syndrome coronavirus 2.

[a]Influenza virus A and B, human parainfluenza viruses 1–4, and respiratory syncytial virus real-time RT-PCR assays were performed on all cases.

[b]Wide-range and specific real-time/conventional PCR assays for bacteria were performed only on the cases that had clinical and/or histopathological suspicion of these infections or if they were positive by immunohistochemical assay.

Mixed infections of other respiratory pathogens were identified in 7 SARS-CoV-2–negative case patients.

the medullary sinuses of a hilar lymph node from an immunosuppressed individual, likely in circulating macrophages (CP 17, Figure 2B1 and 2B2). In 1 case (CP 30), ISH staining demonstrating SARS-CoV-2 RNA was seen within the endothelium, tunica media of vessels, and within vessel lumens in multiple tissues, including in the leptomeninges of the cerebellum, brain stem parenchyma, lung, heart, liver, kidney, and pancreas (Figure 3A, 3B1, and 3B2). SARS-CoV-2 RNA was observed in endothelial cells in the pulmonary vessels, adjacent to a thrombus, from another case patient (CP 22, Figure 3B3 and 3B4). ISH images for positive and negative controls (Supplementary Figure 1) and GAPDH RNA quality control (Supplementary Figure 2*B1* and 2*B2*) are described in the Supplementary Data. The *S*-gene ISH assay was specific for SARS-CoV-2 while *N*-gene ISH assay cross-reacted with both SARS-CoV and SARS-CoV-2 cell culture controls. However, the staining by *N*-gene probe ISH was more abundant compared with the *S*-gene probe ISH.

Histologic findings for 32 SARS-CoV-2 cRT-PCR–positive case patients (Table 3) revealed that 19 of 22 (86%) case patients with available trachea showed tracheitis or tracheobronchitis (Figure 2A1 and 2A3). The most predominant histological feature identified in the lungs of 21 of these 32 (66%) case patients was diffuse alveolar damage (DAD) with various levels of progression and severity, including both exudative and proliferative stages. Interestingly, none of the 4 pediatric case patients had DAD (DOI ≤3 days). Of 32 SARS-CoV-2 cRT-PCR–positive case patients, pulmonary thrombi or emboli were detected in the lungs of 8 (25%), 6 (19%) had mild interstitial pneumonitis, and 10 (31%) had bronchopneumonia. Moderate lymphoplasmacytic myocarditis was seen in 1 case (CP 5) and multifocal lymphohistiocytic and eosinophilic myocarditis was seen in the second (CP 9). However, SARS-CoV-2 RT-PCR and ISH were negative in heart tissues from these patients.

Whole-Genome Sequencing Findings

WGS was performed on respiratory tissues from 27 case patients; we obtained SARS-CoV-2 full and nearly full genome sequences from 19 case patients and partial genome sequences from 7 case patients. WGS did not work for 1 patient. Phylogenetic analysis showed sequences representing all 3 groups (groups A–C) and fall into clades 19A, 19B, 20A, and 20C. Spike amino acid variant D614G was identified in 9 of 26 (35%) case patients; all 9 of them died between 19 March and 1 July 2020. In contrast, all 15 case patients without the D614G variant (with full genome sequences obtained) died between 24 February and 22 March 2020. A summary of common amino acid mutations, along with their respective clades, is described in Supplementary Table 1. No significant amino acid mutation was identified that was consistent within these 19 full genomes. Identical sequences were obtained from the 7 case patients (CP 13–18 and 20) who were part of a long-term care facility outbreak [19].

DISCUSSION

This work provides direct evidence of SARS-CoV-2 replication in lungs and trachea of COVID-19 case patients. SARS-CoV-2 was identified by cRT-PCR in 32 case patients (21 confirmed and 11 suspected) and subgenomic RNA transcripts, demonstrating active viral replication, were detected in lungs or trachea from 17 of 32 RT-PCR–positive case patients. Furthermore, we localized SARS-CoV-2 RNA by ISH in hyaline membranes, pneumocytes, and macrophages of lungs and epithelial cells of airways, and identified cellular targets of SARS-CoV-2 tropism and replication. Replicative viral RNA was detected in lungs

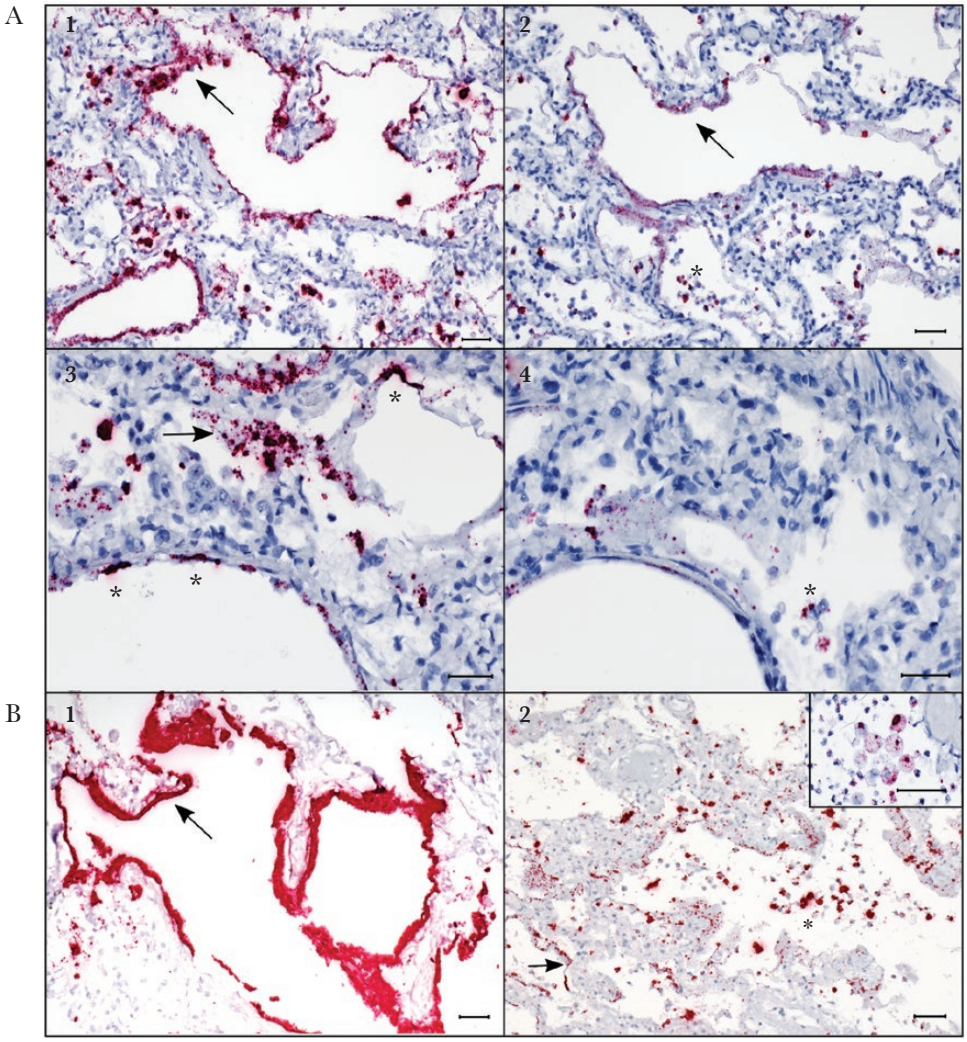

Figure 1. Localization of severe acute respiratory syndrome coronavirus 2 (SARS-CoV-2) RNA in hyaline membranes, pneumocytes, and intra-alveolar macrophages in the lungs of case patients with fatal coronavirus disease 2019 (COVID-19) by in situ hybridization (ISH) assays. *A1*, ISH (in red) targeting the *N*-gene of SARS-CoV-2 strongly stains hyaline membranes lining alveolar spaces (arrow) throughout the lung. Case patient 2. *A2*, ISH targeting the *S*-gene in a serial section from the same case as image *A1*, showing staining in hyaline membranes (arrow), and highlighting staining in intra-alveolar cells consistent with sloughed pneumocytes and alveolar macrophages (asterisk). Case patient 2. *A3*, Higher magnification image showing *N*-gene ISH staining in hyaline membranes (arrow) and pneumocytes (asterisks) lining alveolar spaces in the lung. Case patient 2. *A4*, Serial section from the same case as image *A3*, illustrating staining by ISH targeting the *S*-gene, showing staining in hyaline membranes and scattered staining in intra-alveolar cells (asterisk). Case patient 2. *B1*, Abundant staining by the *N*-gene ISH assay in hyaline membranes (arrow) in the lung of an acute case of COVID-19. Case patient 30. *B2*. Stippled staining by the *N*-gene ISH assay in hyaline membranes (arrow) and strong staining in intra-alveolar cells (asterisk), consistent with sloughed pneumocytes and intra-alveolar macrophages (macrophages highlighted in inset), in the lungs of COVID-19 autopsy cases. Case patients 11 and 23 (inset). All scale markers represent 50 μM.

and trachea within the areas of histopathological changes, suggesting direct virus-induced injury and inflammation.

Importantly, we also demonstrated direct infection of SARS-CoV-2 in vascular endothelium by localizing viral RNA in endothelial cells and tunica media of the vessels in multiple tissues, including lungs, brain stem, cerebellar leptomeninges, heart, liver, kidney, and pancreas. Both case patients with endothelial infection had comorbidities (cardiovascular disease and diabetes) that are characterized by preexisting vascular dysfunction with altered endothelial cell metabolism [28]. Additionally, in 1 of these case patients, SARS-CoV-2 RNA was observed in endothelial cells of the pulmonary vessels, adjacent to a thrombus. In both case patients, relatively lower SARS-CoV-2 rRT-PCR Ct values, consistent with high viral load, was also noted in the lungs. A few recent studies have also reported SARS-CoV-2 infection of endothelial cells using electron microscopy [6, 9]; however, interpretation of electron microscopy is complex [29]. Cellular localization of SARS-CoV-2 RNA in endothelial cells by ISH provides strong evidence of endothelial infection and supports the hypothesis that direct infection of SARS-CoV-2 in endothelial cells may cause vascular dysfunction that leads to hypercoagulation and thrombosis, possibly

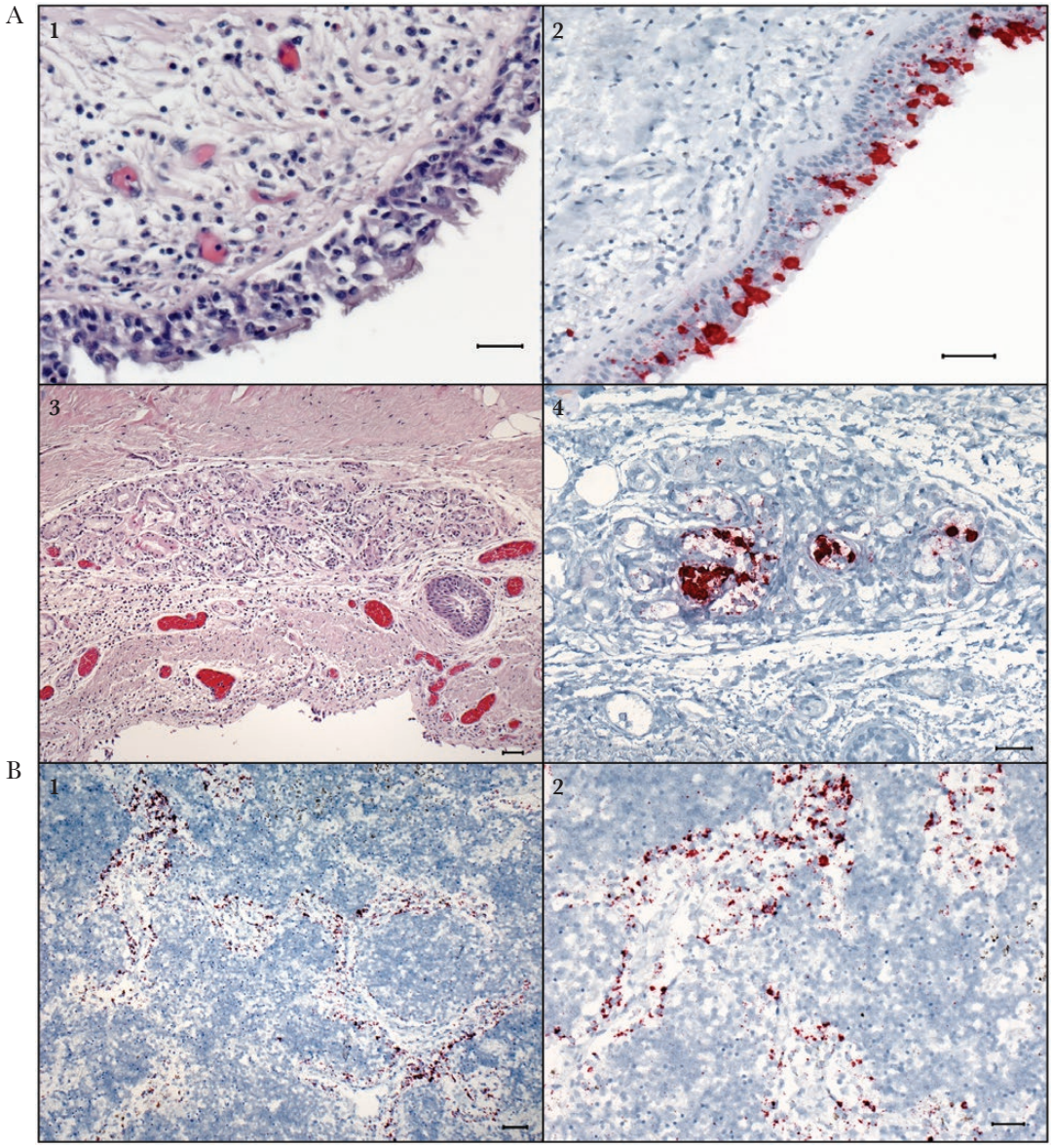

Figure 2. In situ hybridization (ISH) assays demonstrating severe acute respiratory syndrome coronavirus 2 (SARS-CoV-2) RNA in the tracheal epithelium and tracheal submucosal glands, and in macrophages within lymph node of patients with fatal coronavirus disease 2019 (COVID-19). *A1*, Section of trachea showing moderate mononuclear infiltrates in the submucosa of the trachea. Hematoxylin and eosin (H&E) stain. Case patient 12. *A2*, Multifocal, regional ISH staining of respiratory epithelium within the trachea. ISH for *S*-gene of SARS-CoV-2. Case patient 12. *A3*, Photomicrograph of a submucosal gland within the trachea showing mild, mononuclear infiltrates within and around the glands, H&E. Case patient 13. *A4*, ISH staining within the glandular epithelium of the submucosal gland. ISH for *N*-gene of SARS-CoV-2. Case patient 13. *B1*, ISH staining for the N-gene of SARS-CoV-2 within macrophages in the medullary sinuses of the mediastinal lymph node. Case patient 17. *B2*, Higher-magnification image of ISH staining in macrophages within medullary sinuses of the mediastinal lymph node. Case patient 17. All scale markers represent 50 μM.

triggering subsequent immune response and severe disease outcomes. Further investigation into the pathophysiology of virus-induced injury, thrombosis, and associated host inflammatory response is warranted.

Our findings also indicate early tropism and replication of SARS-CoV-2 in the upper respiratory tract. Notably, in SARS-CoV-2 cRT-PCR–positive case patients who had short DOI (1–5 days), active viral replication was detected in trachea of 33% case patients and in lungs of only 17% case patients (Table 3). Conversely, in cRT-PCR–positive case patients with longer DOI (≥10 days), active viral replication was detected in lungs of 69% case patients and in trachea of only 45% case patients (Table 3). In these case patients with longer DOI, lung specimens showed relatively lower SARS-CoV-2 rRT-PCR Ct values in comparison to trachea, suggesting higher viral load in lungs. This may indicate progression of

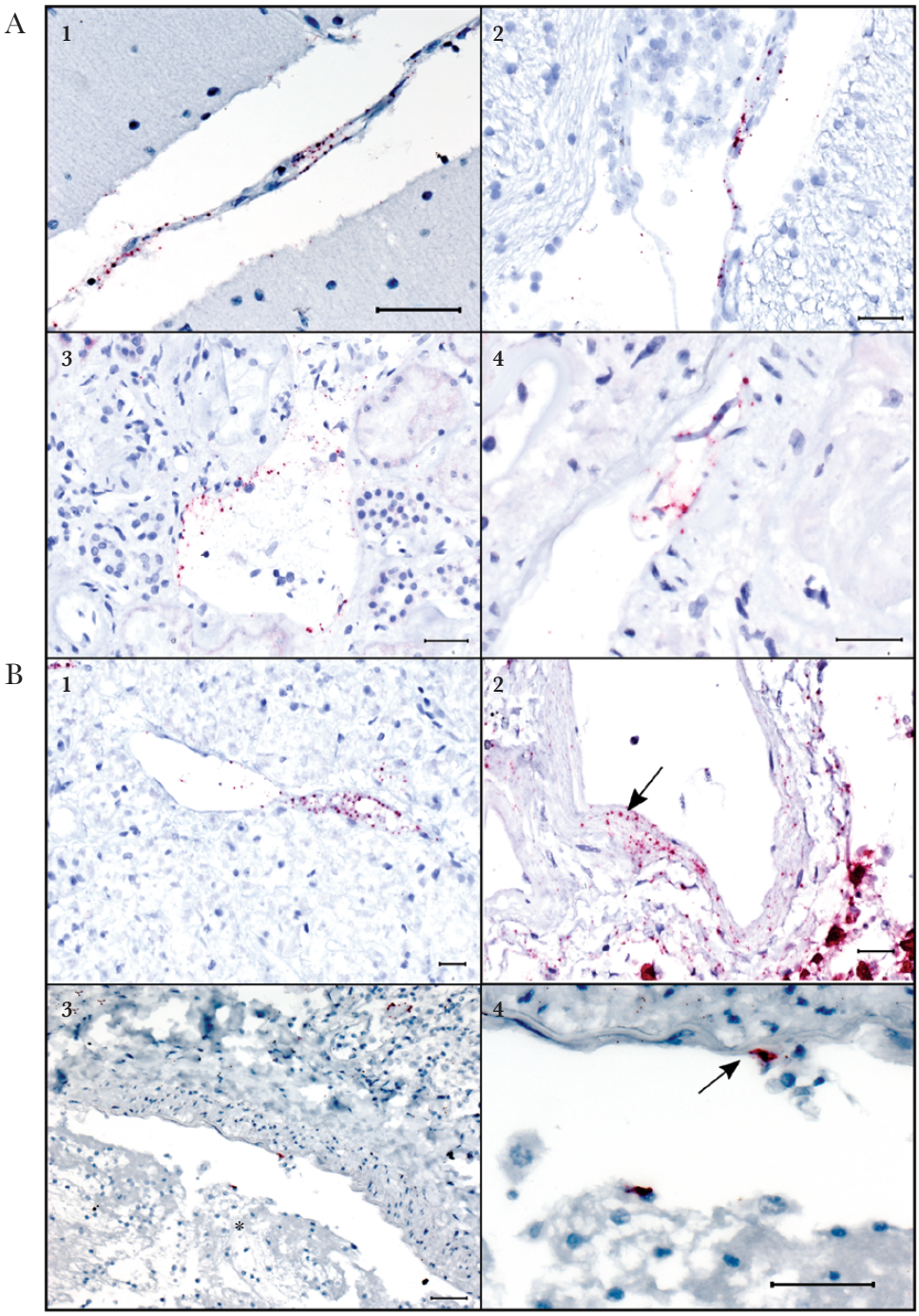

Figure 3. Endothelial and vascular wall staining in multiple tissues by *N*-gene in situ hybridization (ISH) assay in a fatal case of coronavirus disease 2019 (COVID-19) (case patient 30). Also note ISH staining in endothelial cells associated with a thrombus in another COVID-19 fatal case (case patient 22). *A1,* Stippled ISH staining (red) in the endothelium and tunica media of a vessel in the cerebellar leptomeninges in a confirmed case of acute COVID-19. *A2,* Regional staining by ISH in the vascular endothelium and tunica media in the brain stem parenchyma. *A3,* Endothelial ISH staining within vessels in the kidney. *A4,* Stippled ISH staining in detached endothelial cells of a renal vessel. *B1,* Stippled ISH staining seen in the endothelium and tunica media of a vessel within the autolyzed pancreas. *B2,* ISH staining within the tunica media of a vessel in the lung (arrow); ISH staining of pneumocytes in the adjacent alveoli is also noted. *B3,* ISH staining in an endothelial cell and a circulating cell in a thrombosed vessel of an additional confirmed case of COVID-19. Thrombus indicated by an asterisk. *B4,* Higher-magnification image of the distinct endothelial cell staining from image *B3* (arrow). All scale markers represent 50 μM.

infection from airway to lungs over time. Additionally, we noted prolonged detection (up to 26 days) and replication (up to 18 days) of SARS-CoV-2 RNA in the lungs. Similar findings were reported for SARS-CoV in which viral replication was commonly seen in lung tissues up to 20 days after symptom onset [30].

Our histopathological findings show tracheobronchitis in 86% of case patients with trachea available. We also detected viral replication in tracheal submucosal glands of 3 case patients. These findings, along with early tropism and replication in trachea, may help to possibly explaining more efficient transmission of SARS-CoV-2. Our findings in lung tissues from adult case patients support previous autopsy reports, showing DAD as the most prominent finding [10–19]. However, in all 4 pediatric case patients, including 3 infants, a marked absence of DAD was observed in the lungs; all 4 patients had short DOI (≤3 days) and were positive only by RT-PCR. More studies are needed to elucidate the pathogenesis of COVID-19 in children.

We also detected SARS-CoV-2 RNA by cRT-PCR and rRT-PCR in heart, kidney, brain, small intestine, colon, liver, spleen, and pancreas in 14 of 32 respiratory tissue RT-PCR–positive case patients; however, SARS-CoV-2 rRT-PCR Ct values were higher in nonrespiratory tissues than in respiratory tissues (Supplementary Figure 3). Moreover, we did not detect evidence of active viral replication or ISH positivity in nonrespiratory tissues. Thus, SARS-CoV-2 RT-PCR–positive results in nonrespiratory tissues may represent residual genomic viral RNA in blood that was detected by RT-PCR. Higher SARS-CoV-2 RNA levels in blood have been reported in critically ill patients [31]. Another possible explanation of our RT-PCR results could be due to introduction of SARS-CoV-2 RNA from respiratory tissues to nonrespiratory tissues during procurement of postmortem tissues. Some recent studies have identified SARS-CoV-2 RNA by RT-PCR in kidney, colon, spleen, skin, heart, and brain [10, 13, 14]. Nevertheless, extrapulmonary dissemination of SARS-CoV-2 is not well understood.

In addition, we detected coinfection of SARS-CoV-2 with other bacterial or viral pathogens in respiratory tissues of 10 of 32 (31%) cRT-PCR–positive case patients. *Streptococcus* spp, including *S. pneumoniae*, was identified in the lungs of 50% of these 10 case patients; all had histologic evidence of bronchopneumonia. Bacterial coinfections in viral pneumonia are generally associated with increased mortality [32]. Although data are limited, SARS-CoV-2 and community-acquired invasive bacterial coinfection appears to be infrequent [33, 34]. Interestingly, we also detected other pathogens in respiratory tissues from 14 of 32 (44%) SARS-CoV-2 cRT-PCR–negative case patients. Thus, this work highlights the importance of fixed tissue analysis for retrospective diagnosis of infection by SARS-CoV-2 and other respiratory pathogens, particularly for fatal cases in which no previous testing for SARS-CoV-2 was performed. By tissue analysis, we provided the first evidence of SARS-CoV-2 in 11 of 43 (26%) case patients with suspected COVID-19 and identified the first 2 US COVID-19 deaths retrospectively [35]. Furthermore, we performed genetic characterization of SARS-CoV-2 from fixed tissues of fatal cases and identified D614G spike variant in 9 of 26 (35%) RT-PCR–positive case patients. These 9 case patients had a lower median SARS-CoV-2 rRT-PCR Ct value, indicating higher viral load, in lung tissues, in comparison to the 17 case patients without this variant. However, other factors, such as DOI and underlying medical conditions, could also contribute to relatively higher viral load in these case patients. Nonetheless, a recent study showed a correlation between D614G and higher viral load [36].

In summary, this work provides new insights into cellular targets of SARS-CoV-2 tropism and replication, and enhances the understanding of viral pathogenesis, transmissibility, and the mechanisms of severe outcomes of COVID-19, which may have important implications for patient management. SARS-CoV-2 replication in the upper airways during the early disease course, followed by active replication in the lungs for up to 2 weeks, suggests that there may be a wider window of opportunity for interventional antiviral therapy. Furthermore, our work suggests that direct infection of SARS-CoV-2 in vascular endothelial cells may play a crucial role in modulating endothelial dysfunction and thrombosis, triggering subsequent host immune response, and causing vascular complications and severe disease outcomes. Taken together, COVID-19 has a complex pathogenesis and much remains to be explored.

Supplementary Data

Supplementary materials are available at *The Journal of Infectious Diseases* online. Consisting of data provided by the authors to benefit the reader, the posted materials are not copyedited and are the sole responsibility of the authors, so questions or comments should be addressed to the corresponding author.

Notes

Acknowledgments. We sincerely thank the staff of the Centers for Disease Control and Prevention's (CDC) Infectious Diseases Pathology Branch teams, including Epidemiology and Operations, Histology, Immunohistochemistry, Molecular Pathology, and Microbiology teams for accessioning the cases, processing and sectioning the tissues, and preparing the control blocks. We also thank CDC's Natalie Thornburg, Jennifer L. Harcourt, and Azaibi Tamin for providing SARS-CoV-2 culture controls, and Triona Henderson-Samuel for facilitating specimen submission and data collection for the cases. We also gratefully acknowledge the tireless work and support of the CDC COVID-19 Response Teams and thank all state and local health departments, clinicians, pathologists, medical examiners, and coroners who submitted specimens to the CDC.

Disclaimer. The findings and conclusions in this report are those of the authors and do not necessarily represent the official position of the CDC.

Financial support. This work was supported by the Centers for Disease Control and Prevention, Atlanta, Georgia.

Potential conflicts of interest. All authors: No reported conflicts of Interests.

All authors have submitted the ICMJE Form for Disclosure of Potential Conflicts of Interest.

References

1. Zhu N, Zhang D, Wang W, et al. A novel coronavirus from patients with pneumonia in China, 2019. N Engl J Med **2020**; 382:727–33.
2. World Health Organization. Coronavirus disease (COVID-19). https://www.who.int/emergencies/diseases/novel-coronavirus-2019. Accessed 4 January 2021.
3. Centers for Disease Control and Prevention. Coronavirus disease 2019 (COVID-19) in the U.S. https://covid.cdc.gov/covid-data-tracker/#cases_casesper100klast7days. Accessed 4 January 2021.
4. Cevik M, Bamford CGG, Ho A. COVID-19 pandemic—a focused review for clinicians. Clin Microbiol Infect **2020**; 26:842–7.
5. Solomon IH, Normandin E, Bhattacharyya S, et al. Neuropathological features of Covid-19. N Engl J Med **2020**; 383:989–92.
6. Ackermann M, Verleden SE, Kuehnel M, et al. Pulmonary vascular endothelialitis, thrombosis, and angiogenesis in Covid-19. N Engl J Med **2020**; 383:120–8.
7. Wichmann D, Sperhake JP, Lütgehetmann M, et al. Autopsy findings and venous thromboembolism in patients with COVID-19: a prospective cohort study. Ann Intern Med **2020**; 173:268–77.
8. Fox SE, Akmatbekov A, Harbert JL, Li G, Quincy Brown J, Vander Heide RS. Pulmonary and cardiac pathology in African American patients with COVID-19: an autopsy series from New Orleans. Lancet Respir Med **2020**; 8:681–6.
9. Varga Z, Flammer AJ, Steiger P, et al. Endothelial cell infection and endotheliitis in COVID-19. Lancet **2020**; 395:1417–8.
10. Puelles VG, Lütgehetmann M, Lindenmeyer MT, et al. Multiorgan and renal tropism of SARS-CoV-2. N Engl J Med **2020**; 383:590–2.
11. Edler C, Schröder AS, Aepfelbacher M, et al. Dying with SARS-CoV-2 infection-an autopsy study of the first consecutive 80 cases in Hamburg, Germany. Int J Legal Med **2020**; 134:1275–84.
12. Craver R, Huber S, Sandomirsky M, McKenna D, Schieffelin J, Finger L. Fatal eosinophilic myocarditis in a healthy 17-year-old male with severe acute respiratory syndrome coronavirus 2 (SARS-CoV-2c). Fetal Pediatr Pathol **2020**; 39:263–8.
13. Bradley BT, Maioli H, Johnston R, et al. Histopathology and ultrastructural findings of fatal COVID-19 infections in Washington State: a case series. Lancet **2020**; 396:320–32.
14. Hanley B, Naresh KN, Roufosse C, et al. Histopathological findings and viral tropism in UK patients with severe fatal COVID-19: a post-mortem study. Lancet Microbe **2020**; 1:e245–53.
15. Lax SF, Skok K, Zechner P, et al. Pulmonary arterial thrombosis in COVID-19 with fatal outcome: results from a prospective, single-center, clinicopathologic case series. Ann Intern Med **2020**; 173:350–61.
16. Borczuk AC, Salvatore SP, Seshan SV, et al. COVID-19 pulmonary pathology: a multi-institutional autopsy cohort from Italy and New York City. Mod Pathol **2020**; 33:2156–68.
17. Calabrese F, Pezzuto F, Fortarezza F, et al. Pulmonary pathology and COVID-19: lessons from autopsy. The experience of European Pulmonary Pathologists. Virchows Arch **2020**; 477:359–72.
18. Adachi T, Chong JM, Nakajima N, et al. Clinicopathologic and immunohistochemical findings from autopsy of patient with COVID-19, Japan. Emerg Infect Dis **2020**; 26:2157–61.
19. Martines RB, Ritter JM, Matkovic E, et al; COVID-19 Pathology Working Group. Pathology and pathogenesis of SARS-CoV-2 associated with fatal coronavirus disease, United States. Emerg Infect Dis **2020**; 26:2005–15.
20. Bhatnagar J, Blau DM, Shieh WJ, et al. Molecular detection and typing of dengue viruses from archived tissues of fatal cases by rt-PCR and sequencing: diagnostic and epidemiologic implications. Am J Trop Med Hyg **2012**; 86:335–40.
21. Milewska A, Kula-Pacurar A, Wadas J, et al. Replication of severe acute respiratory syndrome coronavirus 2 in human respiratory epithelium. J Virol **2020**; 94:e00957-20.
22. Lu X, Wang L, Sakthivel SK, et al. US CDC real-time reverse transcription PCR panel for detection of severe acute respiratory syndrome coronavirus 2. Emerg Infect Dis **2020**; 26:1654–65.
23. Denison AM, Blau DM, Jost HA, et al. Diagnosis of influenza from respiratory autopsy tissues: detection of virus by real-time reverse transcription-PCR in 222 cases. J Mol Diagn **2011**; 13:123–8.
24. Weinberg GA, Schnabel KC, Erdman DD, et al. Field evaluation of TaqMan Array Card (TAC) for the simultaneous detection of multiple respiratory viruses in children with acute respiratory infection. J Clin Virol **2013**; 57:254–60.
25. Trzciński K, Bogaert D, Wyllie A, et al. Superiority of trans-oral over trans-nasal sampling in detecting *Streptococcus pneumoniae* colonization in adults. PLoS One **2013**; 8:e60520.
26. Shieh WJ, Blau DM, Denison AM, et al. 2009 pandemic influenza A (H1N1): pathology and pathogenesis of 100 fatal cases in the United States. Am J Pathol **2010**; 177:166–75.
27. Paden CR, Tao Y, Queen K, et al. Rapid, sensitive, full-genome sequencing of severe acute respiratory syndrome coronavirus 2. Emerg Infect Dis **2020**; 26:2401–5.

28. Li X, Sun X, Carmeliet P. Hallmarks of endothelial cell metabolism in health and disease. Cell Metab **2019**; 30:414–33.
29. Dittmayer C, Meinhardt J, Radbruch H, et al. Why misinterpretation of electron micrographs in SARS-CoV-2-infected tissue goes viral. Lancet **2020**; 396:e64–5.
30. Nicholls JM, Butany J, Poon LL, et al. Time course and cellular localization of SARS-CoV nucleoprotein and RNA in lungs from fatal cases of SARS. PLoS Med **2006**; 3:e27.
31. Buetti N, Patrier J, Le Hingrat Q, et al. Risk factors for SARS-CoV-2 detection in blood of critically ill patients [manuscript published online ahead of print 2 September 2020]. Clin Infect Dis **2020**. doi:10.1093/cid/ciaa1315.
32. Guo L, Wei D, Zhang X, et al. Clinical features predicting mortality risk in patients with viral pneumonia: the MuLBSTA score. Front Microbiol **2019**; 10:2752.
33. Vaughn VM, Gandhi T, Petty LA, et al. Empiric antibacterial therapy and community-onset bacterial co-infection in patients hospitalized with COVID-19: a multi-hospital cohort study [manuscript published online ahead of print 21 August 2020]. Clin Infect Dis **2020**. doi:10.1093/cid/ciaa1239.
34. Adler H, Ball R, Fisher M, Mortimer K, Vardhan MS. Low rate of bacterial co-infection in patients with COVID-19. Lancet Microbe **2020**; 1:e62.
35. Jorden MA, Rudman SL, Villarino E, et al. Evidence for limited early spread of COVID-19 within the United States, January–February 2020. MMWR Morb Mortal Wkly Rep **2020**; 69:680–4.
36. Korber B, Fischer WM, Gnanakaran S, et al; Sheffield COVID-19 Genomics Group. Tracking changes in SARS-CoV-2 spike: evidence that D614G increases infectivity of the COVID-19 Virus. Cell **2020**; 182:812–27.e19.